International Journal of Thermal Sciences 48 (2009) 1586–1595

Contents lists available at ScienceDirect

International Journal of Thermal Sciences

www.elsevier.com/locate/ijts

Transient numerical analysis of a multi-layered porous heat exchanger including gas radiation effects

S.A. Gandjalikhan Nassab *, M. Maramisaran

Department of Mechanical Engineering, School of Engineering, Shahid Bahonar University, Kerman, Iran

ARTICLE INFO

Article history:
Received 22 May 2008
Received in revised form 15 November 2008
Accepted 18 December 2008
Available online 14 January 2009

Keywords:
Porous heat exchanger
Energy conversion
Gas radiation
Conduction
Convection

ABSTRACT

Thermal characteristics of a new type of multi-layered porous heat exchanger (PHE) are identified in the present study. This system works based on the energy conversion between gas enthalpy and thermal radiation. It has a five-layered structure consisting of two high temperature, two heat recovery and one low temperature sections. These sections are separated from each other by four quartz glass windows. In the two high temperature sections, the enthalpy of high temperature gas flow is converted to thermal radiation that is emitted toward the three adjacent layers where the low temperature air flows are effectively heated by the reverse conversion from thermal radiation into gas enthalpy. The gaseous radiation is also considered, such that in each section, a transient theoretical analysis is conducted for a one-dimensional system where convection, conduction and radiation take place simultaneously in both gas and solid phases. The coupled energy equations for the gas flows and porous layers based on the two-flux radiation model are solved numerically to identify the transient heat transfer characteristics of the system. It is shown that this type of porous heat exchanger has a very high efficiency especially when the porous layers have high optical thicknesses.

1. Introduction

Over the years, porous materials have been used in high temperature systems [1,2]. Several researchers have explored the idea of using high porous materials to capture waste heat from exhaust gases by converting gas enthalpy to thermal radiation [3–5]. One promising method for this energy recovery is to install a radiation shield of porous media normal to the flow direction. A study by Echigo [1] shows that with an appropriate choice of the permeable media, up to 60% of the non-radiating gas energy can be saved.

The effect of gas radiation on the thermal characteristics of an energy recovery system was studied by the first author [6]. In the related paper, it was mentioned that the effect of gaseous radiation is not always small if radiating gases such as carbon dioxide or steam are contained in the working fluid, specially in high temperature condition. In that work, the numerical solution of the coupled energy equations for gas and solid phases was obtained and the crucial influence of gaseous radiation on the system performance was thoroughly explored.

One important property of a porous medium is to have a large value of the surface to volume ratio. Considering this property and based on the energy conversion process between flowing gas enthalpy and thermal radiation by porous medium, a new type of gas-to-gas heat exchanger has been developed by the first author in the previous work [7]. This heat exchanger consists of three porous media separated by two special glass walls, such that the high temperature section is located between two recovery sections. The principle of system's operation is shown in Fig. 1. At the high temperature section, the enthalpy of high temperature gas flow is effectively converted into thermal radiation and the reverse conversion process from thermal radiation into gas enthalpy takes place in the recovery sections. In that study, the steady-state heat transfer characteristics of the proposed heat exchanger was identified.

As a recent study, a series of experiments have been performed by Tomimura et al. [8], to investigate the thermal behavior of a newly proposed multi-layered type of gas-to-gas heat exchanger using porous media. Experiments were done on two-, three- and five-layered heat exchangers under steady condition. As a main result, it was found that the optical thickness of about 8 for the porous layers is enough to obtain sufficient heat recovery rate.

The purpose of the present study, which is follow up the previous work by the first author [7] and also the work of Ref. [8], is to identify the detailed heat transfer characteristics of the newly designed porous heat exchanger (PHE) including gas radiation effects.

The schematic outline of the system is shown in Fig. 2. This PHE is similar to the gas-to-gas heat exchanger which was analyzed in the previous work [7]. It has two high temperature (HT) sections which are located between two heat recovery (HR) and one low

* Corresponding author.
E-mail address: ganjali2000@yahoo.com (S.A. Gandjalikhan Nassab).

1290-0729/$ – see front matter
doi:10.1016/j.ijthermalsci.2008.12.014

Nomenclature

A	surface area
b	back-scattered fraction factor
B	incoming radiation
B'	non-dimensional incoming radiation
c	specific heat
h	heat transfer coefficient
k	effective thermal conductivity
l	characteristic length of porous layer
L	dimensionless group
N_s	number density of solid particles
$Nr_{p,g}$	dimensionless group
$Nu_{p,g}$	dimensionless group
Nl	dimensionless group
Pt	dimensionless group
Pe	Peclet number
q	radiative heat flux
Q	non-dimensional radiative heat flux
R	dimensionless group
R_0	radius of duct
t	time
$T_{p,g}$	porous and gas temperature
T_{g0}	gas temperature at duct's inlet
u	velocity
x	coordinate along the flow direction
x_p	thickness of porous layer
X	non-dimensional coordinate
α	absorption coefficient
ρ	density
θ	non-dimensional temperature
θ_i	inlet ambient temperature
θ_o	outlet ambient temperature
σ	Stefan–Boltzmann constant
σ_s	scattering coefficient
σ_a	absorbing coefficient
σ_e	extinction coefficient, $\sigma_a + \sigma_s$
τ	optical depth, $\sigma_e x$
τ_0	optical thickness, $\sigma_e x_p$
ε	emissivity
ω	scattering albedo
ϕ	porosity
Γ	dimensionless group
T^*	non-dimensional time

Subscripts

g, p	gas and porous, respectively
ht	high temperature section
hr	heat recovery section
lt	low temperature section
n	algebraic summation
s	solid phase
w	wall
1, 2	inlet and exit sections of porous layer
i, o	inlet and outlet

Superscripts

$+, -$	forward and backward directions

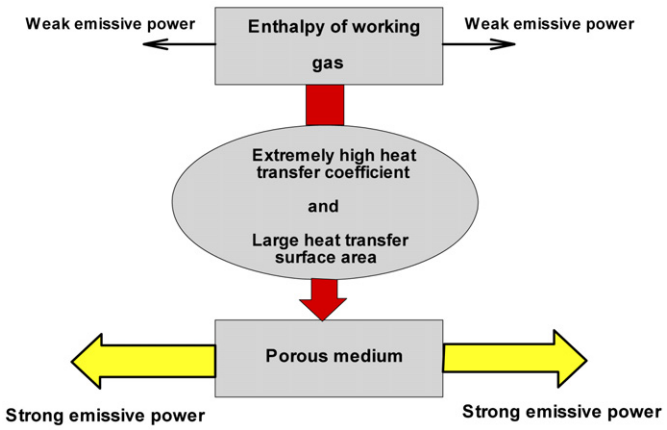

Fig. 1. Effective energy conversion mechanism [1].

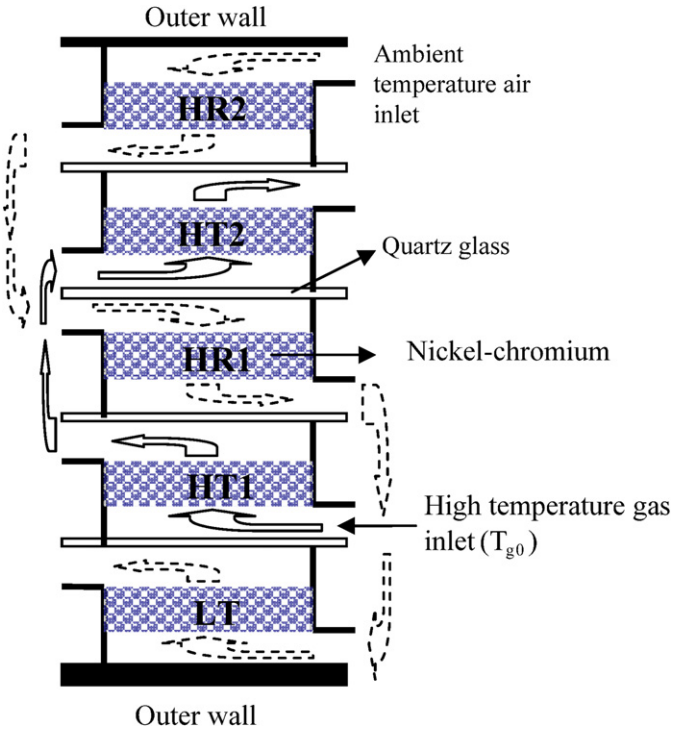

Fig. 2. Geometrical configuration of the porous heat exchanger.

temperature (LT) section. These sections are separated from each other by four quartz glass walls which quite transmit the incident radiative heat flux. The energy conversion from gas enthalpy to thermal radiation occurs in the two HT sections and the reverse process takes place in the HR and LT sections.

In numerical simulation of the PHE, the convection, conduction and radiation heat transfers take place in both solid and gas phases. It should be noted that the effect of gaseous radiation is not always small if the working fluid contains radiating gases such as carbon dioxide or steam, especially at high temperature condition. It is assumed that all of the five porous layers in the PHE are perfectly similar to each other and have the same physical properties.

The governing equations at each section are two energy equations for the gas and solid phases and two radiative transfer equations. The set of equations are solved simultaneously by iterative method to identify the thermal characteristics of the proposed PHE. Besides, an attempt is made to examine the effect of gaseous radiation on the thermal behavior of this heat exchanger.

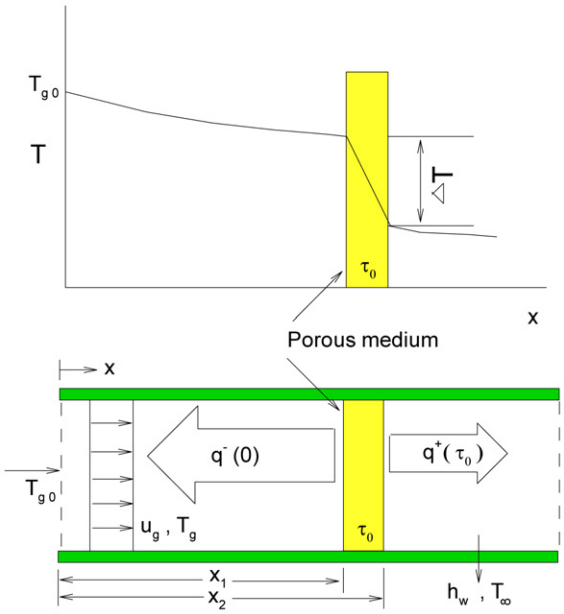

Fig. 3. Schematic sketch of an energy recovery system.

2. Theoretical analysis

2.1. A simple radiative converter system

In all of the sections, the same process which is the energy conversion between gas enthalpy and thermal radiation takes place. Therefore, in the theoretical analysis of each section in the PHE, the governing equations and the numerical procedures are similar to each other. Thereby, only the mathematical analysis of an energy recovery system including a single layer in a duct is described here for space saving.

As illustrated schematically in Fig. 3, when a high temperature gas of T_{g0} flows through a duct, wherein a porous plate with extremely high porosity is installed, a large temperature drop ΔT_g occurs across the porous plate and a large amount of converted radiant energy $q^-(0)$ propagates to the upstream direction of the gas flow.

To analyze the heat recovery system, a one-dimensional high temperature fluid flow passing through a duct with radius R_0 is shown in Fig. 3. Fluid at temperature T_{g0} enters the duct at $x=0$ and the fluid velocity u_g is assumed constant everywhere and the temperature distribution T_g is uniform over every cross section [1–6]. The porous segment which is assumed to be gray body is located between x_1 and x_2 where $(x_1-x_2)=x_p \ll R_0$. Because of the high temperature gas flow, the gaseous radiation is also considered into account. The effective heat transfer coefficient across the duct wall is h_w, i.e., heat exchange with the surrounding environment at T_∞ is equal to $h_w(T_g-T_\infty)$ per unit area. Incoming radiative fluxes from the upstream and downstream sides towards the porous layer are B_1 and B_2, respectively.

2.1.1. Governing equations

Since, the solid and gas are not in local thermal equilibrium, separate energy equations are needed to describe the heat transfer in these two phases. The energy equations for gas and solid phases (Eqs. (1), (2)) along with the radiative heat flux equations based on the two flux radiation model (Eqs. (3), (4)) can be written as follows [6,7]:

$$\begin{aligned}&\phi\rho_g c_g(\pi R_0^2)\left(\frac{\partial T_g}{\partial t}+u_g\frac{\partial T_g}{\partial x}\right)\\&=k_g(\pi R_0^2)\frac{\partial^2 T_g}{\partial x^2}-h_s N_s A_s(\pi R_0^2)(T_g-T_p)\\&\quad-(2\pi R_0)h_w(T_g-T_\infty)\\&\quad+\alpha_g\frac{\partial q_n}{\partial x}(\pi R_0^2)-N_s A_s(\pi R_0^2)(\varepsilon_g\sigma T_g^4-\alpha_g\sigma T_p^4)\end{aligned}\tag{1}$$

$$\begin{aligned}&(1-\phi)\rho_p c_p(\pi R_0^2)\frac{\partial T_p}{\partial t}\\&=k_p(\pi R_0^2)\frac{\partial^2 T_p}{\partial x^2}-(1-\alpha_g)\frac{\partial q_n}{\partial x}(\pi R_0^2)\\&\quad-h_s N_s A_s(\pi R_0^2)(T_p-T_g)\\&\quad+N_s A_s(\pi R_0^2)(\varepsilon_g\sigma T_g^4-\alpha_g\sigma T_p^4)\end{aligned}\tag{2}$$

$$\frac{dq^+}{dx}=-2\sigma_a q^+-2b\sigma_s q^++2\sigma_a\sigma T_p^4+2b\sigma_s q^-\tag{3}$$

$$-\frac{dq^-}{dx}=-2\sigma_a q^--2b\sigma_s q^-+2\sigma_a\sigma T_p^4+2b\sigma_s q^+\tag{4}$$

where

$$q_n=q^+-q^-\tag{5}$$

and $\partial q_n/\partial x$ in gas and porous energy equations deals to the radiation propagation happens in the x-direction. All variables in Eqs. (1) to (5) are defined in the Nomenclature. The governing equations are non-dimensionalized by introducing the following dimensionless parameters:

$$\tau_0=\sigma_e x_p,\qquad \omega=\frac{\sigma_s}{\sigma_e},\qquad B'_{1,2}=\frac{B_{1,2}}{\sigma T_{g0}^4}$$

$$Q_n=\frac{q_n}{\sigma T_{g0}^4},\qquad T^*=\frac{\sigma T_{g0}^3 t}{\rho_p c_p x_p}$$

$$X=\frac{x}{R_0},\qquad Pe=\frac{\rho_g c_g u_g x_p}{k_g}$$

$$Nu_{p,g}=\frac{h_s l}{k_{p,g}},\qquad L=\frac{N_s A_s x_p^2}{l}$$

$$Nl=Nu_g L,\qquad Nr_{p,g}=\frac{k_{p,g}\sigma_e}{\sigma T_{g0}^3}$$

$$R=\frac{\varepsilon_p x_p\sigma T_{g0}^3}{k_p},\qquad Pt=\frac{h_w x_p}{k_g\sigma_e R_0}$$

$$\Gamma=\frac{\rho_p c_p}{\rho_g c_g},\qquad \theta_{p,g}=\frac{T_{p,g}}{T_{g0}}$$

where, Pe is the Peclet number, Nu_g the Nusselt number, l the characteristics length of porous medium (here, the radius of porous layer), Nu_p and Nr_p are the Biot and Planck numbers, respectively. Using the above dimensionless parameters, the non-dimensional forms of the governing equations can be written as follows:

$$\phi\frac{\partial\theta_g}{\partial T^*}=\frac{\Gamma Nr_g}{\tau_0}\begin{bmatrix}\dfrac{\partial^2\theta_g}{\partial X^2}-Pe\,\phi\dfrac{\partial\theta_g}{\partial X}\\-Nl(\theta_g-\theta_p)-2Pt\,\tau_0(\theta_g-\theta_\infty)\\+\alpha_g\Gamma\dfrac{\partial Q_n}{\partial x}-\Gamma L(\varepsilon_g\theta_g^4-\alpha_g\theta_p^4)\end{bmatrix}\tag{6}$$

$$\begin{aligned}(1-\phi)\frac{\partial\theta_p}{\partial T^*}&=-(1-\alpha_g)\frac{\partial Q_n}{\partial X}-\frac{Nr_g Nl}{\tau_0}(\theta_p-\theta_g)+\frac{Nr_p}{\tau_0}\frac{\partial^2\theta_p}{\partial X^2}\\&\quad+L(\varepsilon_g\theta_g^4-\alpha_g\theta_p^4)\end{aligned}\tag{7}$$

$$\frac{dQ^+}{dX}=\tau_0\left[2(1-\omega)(\theta_p^4-Q^+)+2b\omega(Q^--Q^+)\right]\tag{8}$$

$$-\frac{dQ^-}{dX}=\tau_0\left[2(1-\omega)(\theta_p^4-Q^-)+2b\omega(Q^+-Q^-)\right]\tag{9}$$

2.1.2. Boundary conditions

To solve Eq. (6), the following initial and boundary conditions are used.

$$(\theta_g)_{\tau>0} = \theta_\infty \qquad \text{at } T^* = 0$$

$$(\theta_g)_{\tau=0} = \theta_{g0} \qquad \text{at } T^* \geqslant 0$$

$$\left(\frac{\partial \theta_g}{\partial X}\right)_{\tau=\tau_0} = 0 \qquad \text{at } T^* > 0$$

For the porous energy equation, two energy balances at the entrance and exit sections give the following two boundary conditions:

$$\left[\frac{\partial \theta_p}{\partial X} = Nu_p(\theta_p - \theta_g) + R\left(\theta_P^4 - \theta_i^4\right)\right]_{\tau=0} \tag{10}$$

$$\left[-\frac{\partial \theta_p}{\partial X} = Nu_p(\theta_p - \theta_g) + R\left(\theta_P^4 - \theta_o^4\right)\right]_{\tau=\tau_0} \tag{11}$$

and as an initial condition, the following equation is used:

$$(\theta_p)_{\tau\geqslant 0} = \theta_\infty \quad \text{at } T^* = 0$$

Finally, for the two radiative transfer equations, the related boundary conditions are as follows:

$$Q^+(X_1) = B_1' \tag{12}$$

$$Q^-(X_2) = B_2' \tag{13}$$

2.1.3. Solution strategy

Non-dimensional forms of the governing equations are solved numerically to obtain the temperature and radiative heat flux distributions along the porous layer. Eqs. (6) to (9) are coupled through Q^-, Q^+, θ_g and θ_p and have to be solved simultaneously. The finite difference forms of the porous and gas energy equations are obtained using central differencing for space derivative terms where the error of discretization is the order of $(\Delta X)^2$ and the radiative heat flux equations are solved by the forth order Runge–Kutta method. The sequence of calculations at each time step can be stated as follows:

1. A first approximation for temperature and radiative flux distributions is assumed.
2. The discretized form of the gas energy equation is solved by the Thomas-Algorithm to calculate the value of θ_g at each nodal point.
3. The two radiative heat flux equations are solved by the Runge–Kutta method to calculate the radiative flux distributions.
4. The porous energy equation (7) is solved to determine the temperature of solid matrix.

Steps 2 to 4 are repeated until convergence is obtained. This condition was assumed to have been achieved when the fractional changes in the temperature and radiative flux between the two consecutive iteration levels did not exceed 10^{-4} at each grid point. Numerical calculations were performed by writing a computer program in FORTRAN. To obtain the grid-independent solution, the optimum grids of 120 to 150 nodal points based on the optical thickness τ_0 were used in the numerical analysis with the time step of 10^{-3}.

2.2. The porous heat exchanger

As shown in Fig. 2, the porous heat exchanger has a five-layered structure consisting of the HT1, HT2, HR1, HR2 and LT sections. The porous layers in two high temperature sections convert the enthalpy of high temperature gas flow to thermal radiation and in three adjacent porous layers, the reverse conversion process from thermal radiation into gas enthalpy takes place.

For theoretical analysis of this type of heat exchanger, the same method which was used for a single porous layer in a duct can be applied for each porous segment along with the following considerations:

1. Each layer is analyzed individually such that, the one-dimensional coordinate x as an axis along the flow direction is considered for applying theoretical model and computational method.
2. The temperature of inlet gas into the HT1, i.e.,T_{g0} is considered as a reference temperature for all sections.
3. Each layer is located at the entrance of its duct, so the value of x_1 is equated to zero for all layers.

To solve the set of governing equations, the emitted radiations $Q^-(\tau = 0)$ and $Q^+(\tau = \tau_0)$ from each layer behave as incident radiations B_1 and B_2 to the adjacent layers in the PHE. Thereby, at each time step, the coupled set of governing equations for porous layers must be solved iteratively until the steady condition is achieved. The sequence of calculations at each time step can be summarized as follows:

1. A first approximation of incoming radiations B_1' and B_2' to the HT1 and HT2 sections is assumed.
2. The coupled governing equations for the porous layers in HT1 and HT2 sections are solved to calculate the values of Q^-, Q^+, θ_g and θ_p at each nodal point
3. To analyze the HR2 section, the value of B_2' is equated to emitted radiation $Q^+(\tau_0)$ from HT2 (obtained from step 2) multiply to the configuration factor between two adjacent layers. A similar procedure is also considered for the HR1 and LT sections. It should be noted that the value of incident radiation B_1' for both HR2 and LT sections is equal to zero. Because it is assumed that there is not any considerable radiative heat flux from the outer and insulated walls towards these sections.
4. By these computations, the incoming radiations B_1' and B_2' which have been assumed in step 1 will be corrected.
5. Steps 2 and 3 are repeated until all calculated variables satisfy certain imposed convergence criteria.

3. Validation of the computational results

In order to confirm the validity of the numerical results, a heat recovery system as an unique and independent apparatus is analyzed in a test case and the numerical results in steady condition are compared with theoretical predictions in Ref. [9]. In this system, a large amount of incident radiation B_1 is effectively converted to gas enthalpy. This process is exactly opposite to that shown in Fig. 3, in which the gas enthalpy is converted into thermal radiation.

The steady-state gas and porous temperature distributions are presented in Fig. 4. As this figure shows, the porous temperature at inlet section increases sharply as a result of absorbing the incoming radiation and the low temperature gas flow is effectively heated by convective heat transfer between gas and solid phases. However, Fig. 4 shows a good consistency between the present results and those obtained theoretically in Ref. [9].

Since, the numerical results of Fig. 4 are in steady condition, another test case is also analyzed to validate the transient computational results and a comparison is made with the theoretical and experimental data in Ref. [4]. The system under consideration is a heat recovery system in which the gas enthalpy is converted into thermal radiation as it was shown in Fig. 3. In the studies by

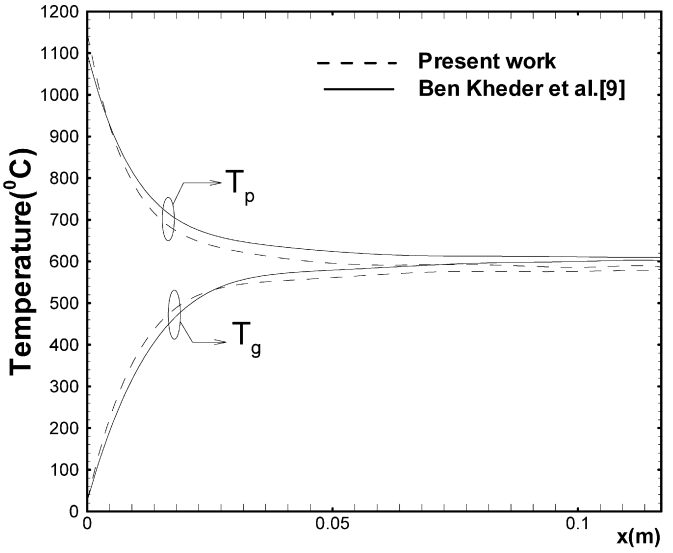

Fig. 4. Gas and porous temperature distributions along the porous media in steady condition. $\theta_\infty = 1$, $B'_1 = 14152$, $B'_2 = 0$, $\omega = 0$, $\tau_0 = 1$, $R = 0.1$, $\Gamma = 3077$, $Pe = 18$, $Nl = 45630$, $Nu_p = 8.18$, $Nr_p = 80$, $Nr_g = 0.32$, $Pt = 0$, $\alpha_g = \varepsilon_g = 0$.

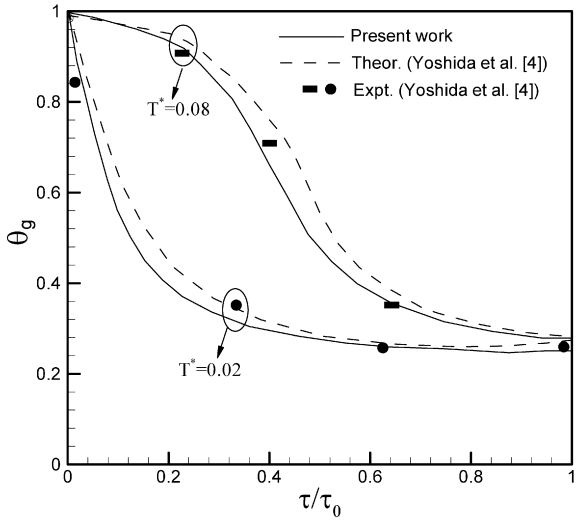

Fig. 5. Time history of gas temperature inside the porous segment. $\theta_\infty = 0.3$, $B'_1 = 0.885$, $B'_2 = 0.006$, $\omega = 0$, $\tau_0 = 20$, $\Gamma = 3120$, $Pe = 153$, $Nl = 9120$, $Nr_p = 0$, $Nr_g = 1.09$, $Pt = 0$, $\alpha_g = \varepsilon_g = 0$.

Yoshida et al. [4], experiments were performed in order to confirm the validity of the theoretical analysis.

Fig. 5 shows the variation of gas temperature along the porous layer at two different time steps. It can be seen that the gas temperature decreases in the flow direction, especially at the entrance of porous layer and in the initial time periods. However, this figure shows a good consistency between theory and experiment.

4. Results and discussion

As illustrated schematically in Fig. 2, the thermal behavior of the new type of five layered PHE which works based on the energy conversion between gas enthalpy and thermal radiation is analyzed here. All of the five layers have a same radius equal to R_0 and the spacing between two adjacent layers is equated to $R_0/4$, which gives the configuration factor of 0.8.

Four quartz glass windows are used for separating the porous layers from each other. Since, the temperature of porous layers is not too high, a great part of radiated energy from porous media lies in the range of long wavelength (infrared). It should be noted that the range of wavelengths in thermal radiation is from about 0.1 to 100 μm, therefore a special glass type as a Hoya R-72 IR filter which passes completely the wave lengths of 720 nm and above is a good choice for this application [7]. Regarding to the high transparency of this glass type for thermal radiation, it is assumed in the computations that the whole incident radiation toward the glass walls are quit transmitted without any reflection, absorption and emission.

There are many independent parameters in analyzing this PHE, but it is possible to present only some results for a wide range of conditions. The values of dimensional and non-dimensional parameters in the computations of the following results (Figs. 6 to 8) have been given in Tables 1 and 2, respectively. The porous media is considered non-scattering, except in Fig. 10(a) in which the effect of scattering is considered.

The gas and porous temperature profiles θ_g and θ_p, and also the variation of radiative fluxes Q^+ and Q^- along the layers with $\tau_0 = 1$ at different five sections in steady condition are shown in Fig. 6. It can be seen that in the HT1 and HT2 sections, the gas enthalpy is converted into thermal radiation because of the sharp temperature decrease in the gas flow. The porous layers in the HR and LT sections are heated by absorbing the incoming radiations from two HT sections and the low temperature air flow is effectively heated in three steps by passing through HR2, HR1 and LT sections, respectively.

It is seen that in all of sections, the gas and porous temperatures are near to each other due to the large convection coefficient with this reality that the gas temperature is greater than the temperature of porous media in the HT1 and HT2 and the reverse state is seen in the HR1, HR2 and LT sections. In this test case, if the temperature of inlet working hot gas be equal to 1000 K, this type of heat exchanger causes a temperature increase in air flow of about 200 K. Therefore, this type of heat exchanger is very useful for practical application as an efficient air heater. It should be mentioned that in the computations of Fig. 6, the gas radiation effect is neglected.

In order to show the transient behavior of the PHE along with the effect of gas radiation, the gas temperature distributions in the HT1 and LT sections are shown in Figs. 7(a) and 7(b) with and without considering gas radiation and in several different times from the start of the system's operation up to the steady condition. A very sharp temperature decrease is seen in the initial time period in the HT1 section. Therefore, this section behaves as a perfect insulator in the start of system's operation by converting a great amount of gas enthalpy into thermal radiation. In the time periods near to steady condition, a decrease in the amount of gas enthalpy drop is evident. Furthermore, it is seen that the gas radiation causes a decrease in the enthalpy drop specially in the initial time periods. In the LT section, an apposite behavior is seen from Fig. 7(b), such that in the initial time periods, there is a small increase in the air temperature and after spending some seconds, the temperature increase in air flow enhances. Additionally, it is seen that the gas radiation improves the LT performance by more increasing the gas temperature inside this section in comparison to the non-radiating condition.

The effect of gas radiation on thermal behavior of the PHE is also shown in Fig. 8 by drawing the gas temperature and radiative heat flux distributions along different sections in steady condition. There is not a considerable effect of gas radiation on the temperature and radiative heat flux in steady condition, but the numerical results indicates that the gas radiation effect causes a significant decrease in the time of steady state.

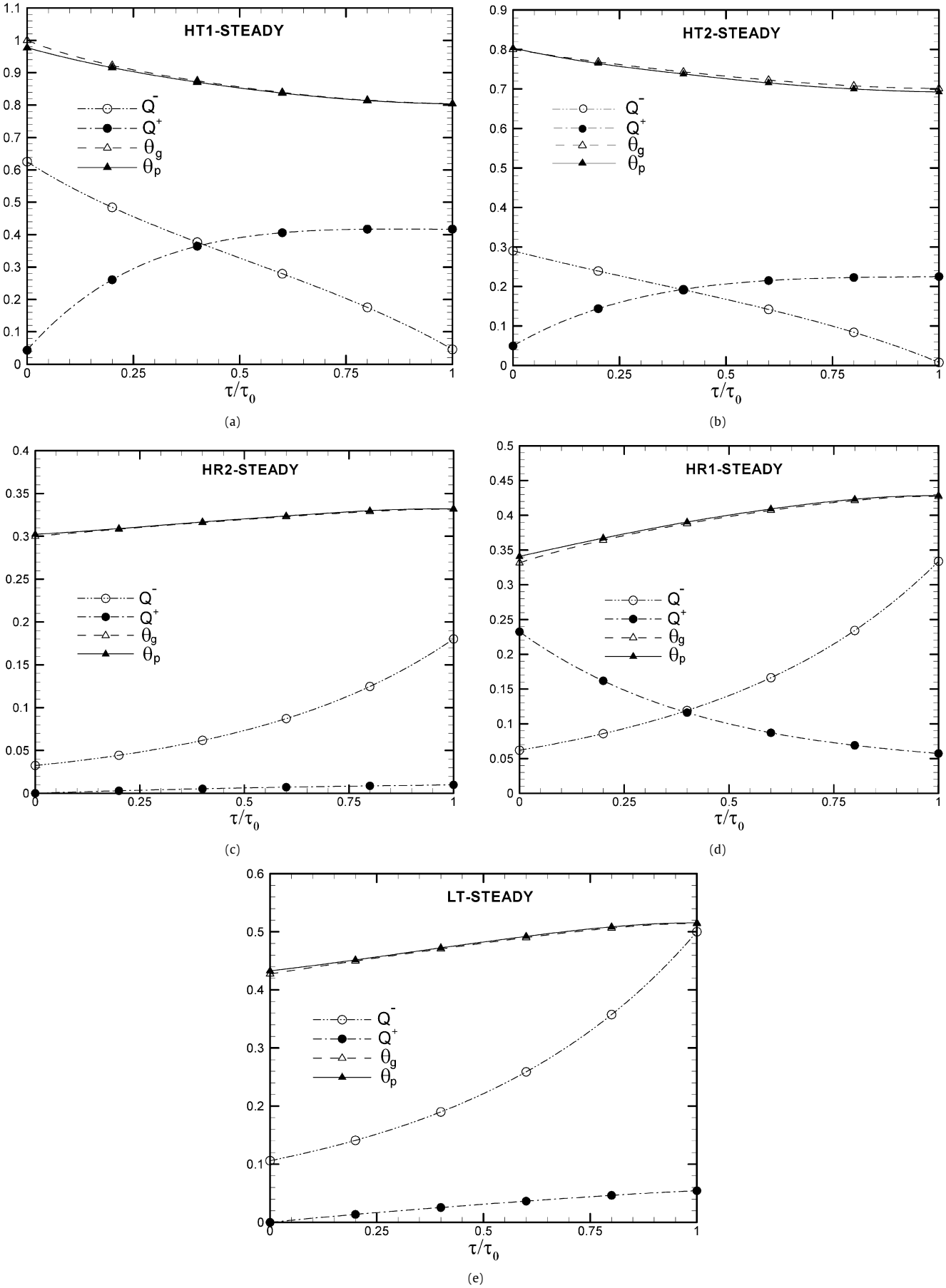

Fig. 6. Distribution of gas and porous temperatures and radiative heat flux inside the layers in steady condition. (a) HT1, (b) HT2, (c) HR2, (d) HR1, (e) LT.

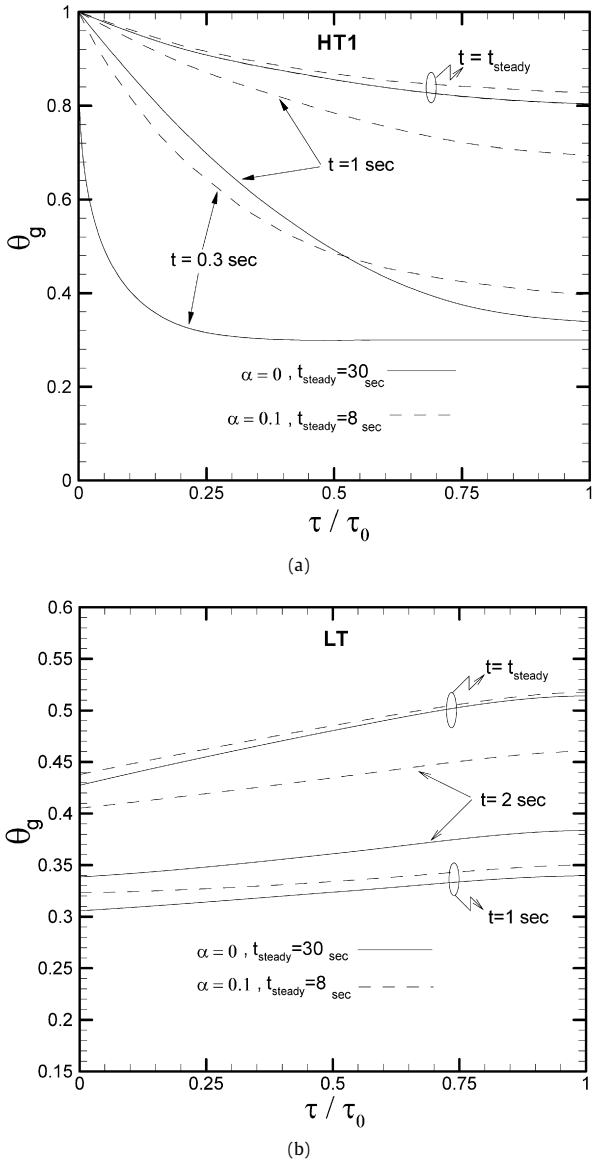

Fig. 7. Transient gas temperature distributions in the HT1 and LT sections. (a) Gas temperature distribution in the HT1 section. (b) Gas temperature distribution in the LT section.

Fig. 9 shows an example of the inlet and outlet gas temperatures in each section of the five-layered heat exchanger for 727 °C (1000 K) level of $T_{\mathrm{ht1},i}$. Each section corresponds to the space between the vertical lines which symbolically represents the separating wall, insulated wall and outer wall. The arrow represents the flow directions of the high or low temperature gases in the HT1, HT2, HR2, HR1 and LT sections. Numerical results show that the maximum and minimum rates of heat transfer between porous layer and gas flow take place in HT1 and HR2 sections, respectively. Fig. 9 indicates that by increasing optical thickness, the temperature drop of incoming hot gas ($T_{\mathrm{ht1},i}$) where exits from the HT2 section, has been increased and the incoming cool air where finally exits from the LT section, has been recovered more heating energy from heat exchanger. Thereby, using of porous layers with large optical thicknesses in the PHE construction improves the system performance. It should be mentioned that in the computations of Fig. 9, the gas radiation effect is considered with $\varepsilon_g = \alpha_g = 0.1$ and the values of non-dimensional parameters are the same as in Table 2, except for the cases with $\tau_0 = 2$ and 7.

Table 1
The values of dimensional parameters.

Parameter	Unit	Value
ρ_p	kg/m^3	1824
ρ_g	kg/m^3	1.2
c_p	kJ/kg °C	0.594
c_g	kJ/kg °C	1.28
u_g	m/s	64
k_p	W/m °C	0.813
k_g	W/m °C	0.133
h_s	W/m^2 °C	56
$A_s N_s$	m^{-1}	9.61×10^3
R_0	m	0.15
x_p	m	0.011
σ_e	m^{-1}	95
T_{g0}	°C	727

Table 2
The values of non-dimensional parameters.

Parameters	Values
θ_∞	0.3
τ_0	1
R	0.77
Γ	705
Pe	8.143
Nl	489
L	7.75
Nr_p	1.365
Nr_g	0.22
Nu_p	10.33
Pt	0
ϕ	0.95
$\alpha_g = \varepsilon_g$	0, 0.05, 0.1

Fig. 10 shows the effect of τ_0, ω and the inlet gas temperature T_{g0} on the PHE efficiency which is defined generally by the following equation:

$$\eta = \frac{\sum_{\mathrm{LT,HR1,HR2}} \dot{m}_a c_a \Delta T_a}{\dot{m}_g c_g (T_{g0} - T_\infty)} \tag{14}$$

Here, $\dot{m}_a$, $\dot{m}_g$, c_a and c_g are the mass flow rate and the specific heat at constant pressure of the air and gas flows, respectively. ΔT_a is the air temperature increase along HR1, HR2 and LT sections and T_{g0} is the inlet gas temperature into the HT1 section. Since in the computations, the physical properties and velocity of the gas and air flows are considered equal to each other, the dimensionless form of the above equations can be stated as follows:

$$\eta = \frac{\sum_{\mathrm{LT,HR1,HR2}} \Delta\theta_a}{(1 - \theta_\infty)} \tag{15}$$

It should be noted that in the computations of Fig. 10, the gas radiation effect is considered with $\varepsilon_g = \alpha_g = 0.1$. It is seen from Fig. 10(a) that the PHE efficiency increases by increasing the optical thickness of porous layers such that the optical thickness of about 3 seems enough to obtain the sufficient efficiency. The effect of radiative scattering on the PHE efficiency is also shown in Fig. 10(a). It is seen that radiative scattering causes a decrease in the efficiency of PHE specially for large optical thicknesses. The effect of T_{g0} on the efficiency of PHE is also shown in Fig. 10(b). The PHE efficiency increases when the temperature of inlet gas flow into the HT1 section becomes very high especially in the case of large optical thicknesses. However, it is seen from Fig. 10 that this type of porous heat exchanger has a very high efficiency which is higher than the conventional ones with the maximum efficiency of about 25% [8].

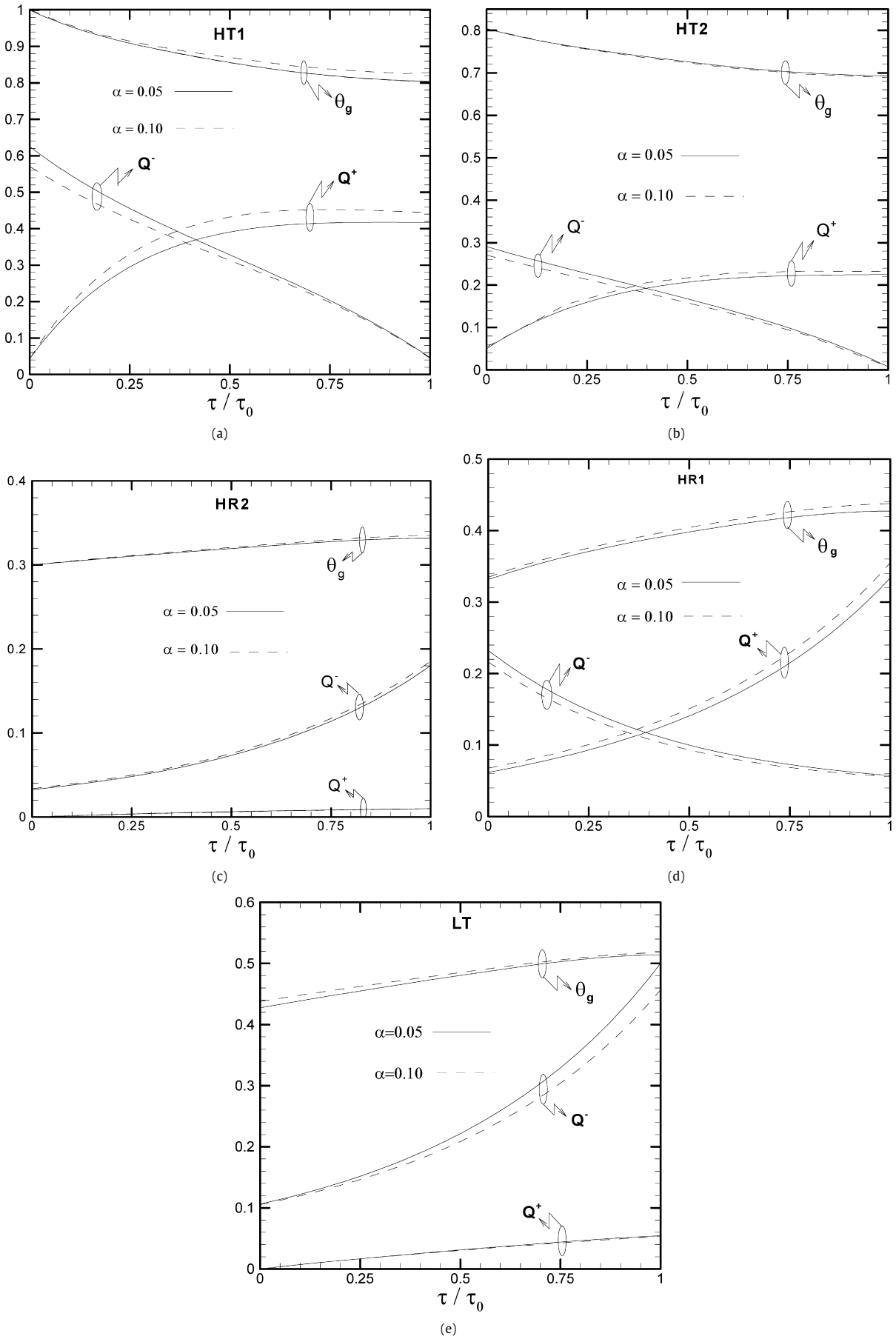

Fig. 8. Distribution of gas temperature and radiative heat flux inside the layers in steady condition. (a) HT1, (b) HT2, (c) HR2, (d) HR1, (e) LT.

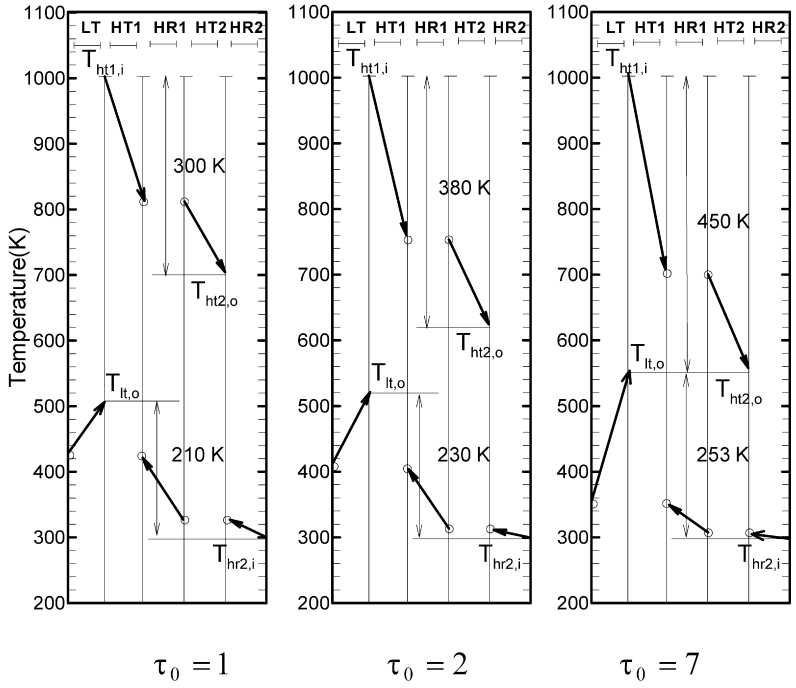

Fig. 9. Example of temperature distributions in each section.

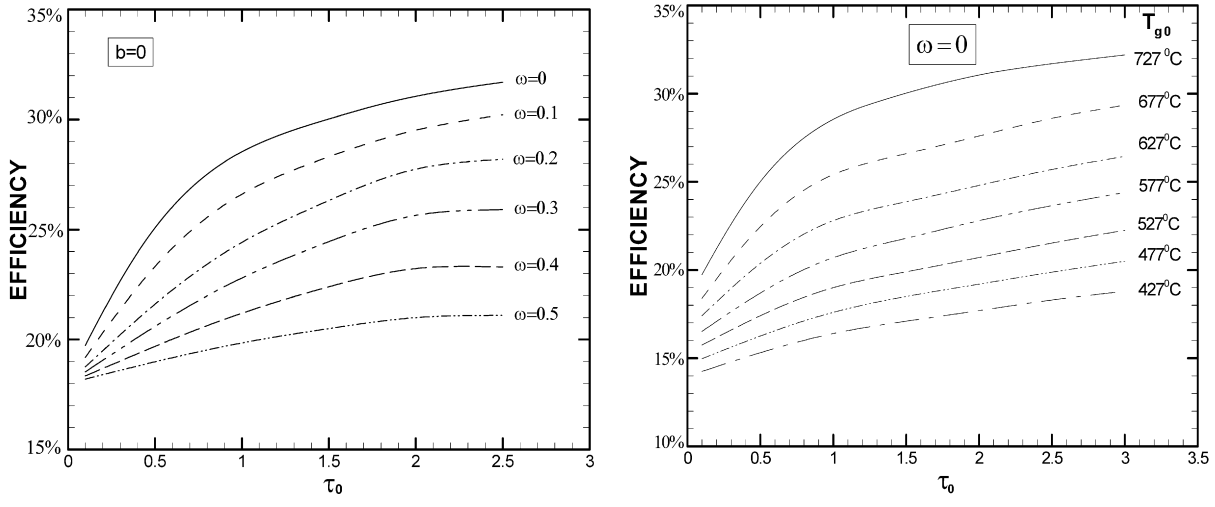

Fig. 10. Effect of τ_0, ω and T_{g0} on the PHE efficiency. (a) Variation of PHE efficiency with τ_0 at different values of ω. (b) Variation of PHE efficiency with τ_0 at different values of T_{g0}.

5. Conclusion

A numerical study has been performed on a new type of PHE to identify the thermal characteristics of this system in transient condition with considering the effect of gaseous radiation. The heat exchanger works based on the energy conversion phenomena between gas enthalpy and thermal radiation by porous media. The heat transfer behavior of the newly proposed PHE is investigated by solving the governing equations in transient condition and the two-flux model is used to describe the radiative fluxes from the solid matrix. The crucial influence of gaseous radiation on thermal behavior of the PHE is thoroughly explored. Results show that the gas radiation does not have a considerable effect on the steady state thermal behavior of PHE such that this effect is much more in the starting time period of the system's operation. Also, the effect of gas radiation causes a significant decrease in the time to reach steady state. However, computational results show a very high efficiency for this type of PHE specially, when the porous layers with large optical thicknesses and small scattering coefficients are used in the construction of this system.

References

[1] R. Echigo, Effective energy conversion method between gas enthalpy and thermal radiation and application to industrial furnaces, in: Proc. 7th Int. Heat Transfer Conf., München, vol. 6, 1982, pp. 361–366.

[2] R. Echigo, Heat transfer augmentation in high temperature heat exchangers, in: High Temperature Equipment, Hemisphere, Washington, DC, 1986, pp. 41–72.

[3] K.Y. Wang, C.L. Tien, Thermal insulation in flow systems combined radiation and convection through a porous segment, J. Heat Transfer 106 (1984) 453–459.

[4] H. Yoshida, J.H. Yung, R. Echigo, T. Tomimura, Transient characteristics of combined conduction, convection and radiation heat transfer in porous media, Int. J. Heat Mass Transfer 33 (5) (1990) 847–857.
[5] S.A. Gandjalikhan Nassab, Transient heat transfer characteristics of an energy recovery system using a porous medium, in: Proc. Instn. Mech. Engrs., Part A, J. Power and Energy 216 (2002) 387–394.
[6] S.A. Gandjalikhan Nassab, M. Fallah, Study of energy recovery by means of porous media considering gas radiation effect, in: Proc. Instn. Mech. Engrs., Part A, J. Power and Energy 220 (2006) 509–513.
[7] S.A. Gandjalikhan Nassab, Effective gas-to-gas heat exchanger by means of energy conversion between gas enthalpy and thermal radiation, in: Proc. Instn. Mech. Engrs., Part A, J. Power and Energy 218 (2004) 451–457.
[8] T. Tomimura, K. Hamano, Y. Honda, R. Echigo, Experimental study on multilayered type of gas-to-gas heat exchanger using porous media, International Journal of Heat and Mass Transfer 47 (2004) 4615–4623.
[9] C. Ben kheder, B. Cherif, M.S. Sifaoui, Numerical study of transient heat transfer in semitransparent porous medium, Renewable Energy 27 (2002) 543–560.